JACS Au
AN OPEN ACCESS JOURNAL OF THE AMERICAN CHEMICAL SOCIETY

pubs.acs.org/jacsau
Article

Revealing the Ultrafast Energy Transfer Pathways in Energetic Materials: Time-Dependent and Quantum State-Resolved

Jia Liu, Jitai Yang, Gangbei Zhu, Jiarui Li, You Li, Yu Zhai, Huajie Song,* Yanqiang Yang,* and Hui Li*

Cite This: *JACS Au* 2024, 4, 4455−4465

Read Online

ACCESS | Metrics & More | Article Recommendations | Supporting Information

ABSTRACT: Intramolecular vibrational energy transfer is gaining tremendous attention as a regulator of condensed-phase behavior and reactions. In polyatomic molecules, this transfer is an ultrafast process involving multiple modes with numerous quantum states. The inherent complexity and rapid evolution of these processes pose significant challenges to experimental observation, and the high computational costs make full quantum mechanical calculations impractical with current technology. In the intramolecular energy transfer process, whether the doorway modes are intermediaries for transferring energy from lattice phonons to high-frequency intramolecular vibrational modes has been a controversial issue. However, the broad range of doorway modes complicates the experimental identification of a specific doorway in the transfer process corresponding to a specific end point. Here, for the first time, we utilize a combination of vibrational projection, statistical analysis, and the local quantum vibrational embedding (LQVE) method to elucidate the ultrafast energy transfer pathways that upconvert energy from lattice phonons to intramolecular modes in the typical energetic material β-HMX. This approach enables us to resolve the coupled vibrational mode groups, identify the most probable energy transfer pathways corresponding to the different final modes, and clearly confirm that the doorway region is a mandatory pathway for energy transfer. The LQVE method's time-dependent and quantum state-resolved advantages are leveraged to reveal the microscopic mechanism of the energy transfer process. The time scale of these processes is determined at about 1 ps, and the first theoretical two-dimensional infrared spectroscopy evidence is provided, which is confirmed by the experimental results. These findings deliver important insights into the fundamental mechanisms of ultrafast energy transfer in energetic materials, providing theoretical support for controlling explosive behavior and designing new explosives. The methodologies developed in this work can be extended to other condensed phase materials and used to evaluate the coupling between multiple vibrational modes.

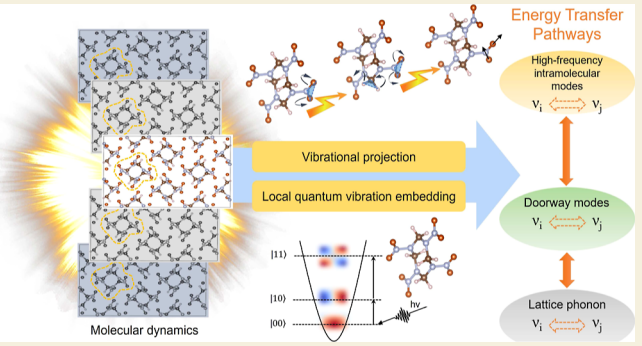

KEYWORDS: *energy transfer pathways, vibrational mode, local quantum vibration embedding, state population relaxation, two-dimensional infrared spectroscopy, β-HMX*

1. INTRODUCTION

Vibrational energy transfer (VET) is a pivotal process that governs the dynamics and reactions of solutions and other condensed phases. Of particular interest is the intramolecular vibrational energy redistribution (IVR), where energy flows between different vibrational modes within a molecule. This process often competes with other chemical events[1] and has been a major focus of study for several decades.[2,3] A series of seminal works have been dedicated to understanding the nature of IVR across a variety of materials, with the aim of utilizing or controlling this process.[4−9] In particular, studies have shown that the stability, reactivity, and detonation properties of energetic materials are significantly affected by intramolecular vibrational energy transfer.[10] Consequently, precisely controlling the IVR process in these materials is of critical importance.

In the multiphonon up-pumping model,[11,12] it is posited that certain regions of frequencies, known as doorway modes, play a critical role in the overall energy transfer process. According to this model, when a crystal experiences mechanical shock, excess energy is initially transferred from lattice phonons to the doorway modes. The energy is then further channeled from the doorway modes to high-frequency internal vibrational modes, where it is rapidly redistributed until it converges on specific modes that are crucial for bond breaking and subsequent detonation reactions.[13,14] However, this model is not without controversy. Some studies have validated this model; for instance, Kumar et al. employed Fermi's golden rule-based 3-

Received: August 28, 2024
Revised: November 5, 2024
Accepted: November 7, 2024
Published: November 13, 2024

https://doi.org/10.1021/jacsau.4c00775
JACS Au 2024, 4, 4455−4465

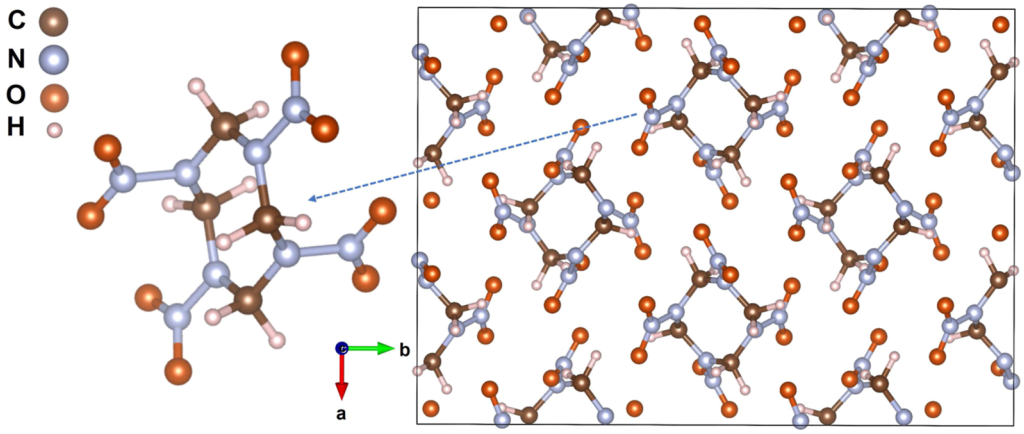

Figure 1. 2 × 2 × 2 β-HMX supercell and the probe molecule.

phonon theoretical analysis to analyze energy up-pumping in 1,3,5-trinitroperhydro-1,3,5-triazine (RDX),[15] and Bondarchuk proposed a method to calculate the energy transfer rates of such multiphonon up-pumping for both isolated molecules and crystalline materials.[16] In contrast, some researchers have suggested that energy transfer occurs directly, with lattice phonons predominantly governing thermal energy transfer rather than being mediated through doorway modes.[17,18] This ongoing debate highlights the unresolved nature of the energy transfer pathways.

Recent studies have provided valuable insights into the time scales of energy transfer in energetic materials. For instance, Cole-Filipiak and Ramasesha et al. identified $a \sim 100$ ps (ps) time scale in pentaerythritol tetranitrate (PETN), RDX, and 2,4,6-triamino−1,3,5-trinitrobenzene (TATB), which was mediated by lattice vibrations, providing strong evidence for coupled vibrations in these systems.[19,20] Ostrander et al. observed a specific energy transfer pathway in PETN with a time scale of 2 ps.[21] Similarly, Shi et al. identified an energy dissipation pathway related to Davydov splitting in the microcrystalline form of cyclic nitramine hexahydro-1,3,5-trinitro-*s*-triazine (HHTT).[22] Yang et al. further discovered intramolecular energy transfer between the axial and equatorial nitro groups in β-octahydro-1,3,5,7-tetranitro-1,3,5,7-tetrazocine (β-HMX) occurring on the picosecond time scale.[23] Despite these advancements, it remains a significant challenge to experimentally elucidate the intricate details of IVR in energetic materials, primarily due to the ultrafast and complex nature of the process, which involves multiple modes and numerous quantum states.

Theoretical calculations have proven useful in providing more detailed insights into the IVR process, offering explanations for VET and IVR dynamics.[15,20,24,25] However, due to the challenges of performing full quantum mechanical (QM) calculations, most studies have relied on classical mechanics. While these classical approaches have advanced our understanding, they fall short in accurately describing high-frequency vibrational modes, where quantum effects play a crucial role.

In this study, we propose an integrated approach combining vibrational projection, statistical analysis, and the local quantum vibrational embedding (LQVE) method to investigate the IVR process. The LQVE method is an advancement of our previously developed quantum vibrational perturbation (QVP) method,[26,27] which utilizes quantum mechanics to determine instantaneous physical quantities such as instantaneous vibrational frequency, dipole, polarization, etc. This method incorporates the effects of surrounding molecular clusters as well as the vibrational modes of the probe molecule, which were previously unexplored as environmental influences. The LQVE method provides time-dependent vibrational frequencies at a semiclassical level, addressing the high computational demands of full quantum mechanical calculations and the limitations of classical mechanical calculations in terms of accuracy.

2. METHODOLOGY

2.1. Vibrational Projection Method and Applications

The structure of the in-crystal probe molecule varies during the molecular dynamics (MD) simulation. Projecting the instantaneous Cartesian coordinates onto the vibrational mode coordinates allows for a better view of the correlation between vibrational modes.

2.1.1. Vibrational Projection. In-crystal molecules can better account for the effects of the crystalline environment compared to isolated molecules in the gaseous state. Figure 1 depicts the β-HMX supercell, and a specific in-crystal molecule is chosen as a probe molecule in this study. The partial Hessian approach[28−30] is utilized to obtain the vibrational modes of the probe molecule by (1) optimizing the supercell to reach the global minimum of the potential energy surface (PES) to get equilibrium coordinates, where the coordinates of each β-HMX molecular are denoted as $\boldsymbol{x}_e$, and we assume that its center of mass is located at the origin of the coordinate system, then (2) computing the (mass-weighted) Hessian of the supercell and slicing out the partial Hessian of a probe molecule, and finally (3) performing diagonalization to obtain the vibrational modes coordinates ξ_s. Note that the orientations of ξ_s and $\boldsymbol{x}_e$ have to consist and are fixed in the following procedures.

To track the vibrational motion of molecules, we projected the mass-weighted Cartesian coordinates onto the vibrational modes.[31,32] The mass-weighted vibrational mode coordinates of vibrational mode i are given by

$$\tilde{Q}_i = \tilde{\boldsymbol{\xi}}_i \cdot (\mathbf{U}^{\mathrm{T}} \cdot (\tilde{\boldsymbol{x}}(t) - \tilde{\boldsymbol{t}}) - \tilde{\boldsymbol{x}}_{\mathrm{e}}) \tag{1}$$

where $\boldsymbol{t}$ is the translation vector, which can be determined by computing the displacement between the center of mass of $\boldsymbol{x}$ and that of $\boldsymbol{x}_e$. $\mathbf{U}$ is the rotation matrix obtained by the Kabsch algorithm,[33−35] which minimized the root mean squared difference (RMSD) between the mass-weighted coordinates, $\tilde{\boldsymbol{x}}_{\mathrm{e}}$ and $\tilde{\boldsymbol{x}} - \tilde{\boldsymbol{t}}$.

https://doi.org/10.1021/jacsau.4c00775
JACS Au 2024, 4, 4455−4465

2.1.2. Vibrational Mode Coupling Analysis. To our knowledge, most of the widely used trajectory analysis software analyzes the distribution function based on the internal coordinates. In this work, we propose a vibrational mode coordinate-based combined distribution function (CDF) to study the correlations between vibrational modes. We make two-dimensional correlation of projections Q_{s_1} and Q_{s_2} as

$$C(Q_{s_1}, Q_{s_2}) = \frac{\rho^{2D}(Q_{s_1}, Q_{s_2}) - \rho^{1D}(Q_{s_1}) \otimes \rho^{1D}(Q_{s_2})}{\rho^{2D}(Q_{s_1}, Q_{s_2})} \tag{2}$$

in which $\rho^{2D}(Q_{s_1},Q_{s_2})$ is the 2D density distribution function of Q_{s_1} and Q_{s_2}, whereas $\rho^{1D}(Q_{s_1})$ and $\rho^{1D}(Q_{s_2})$ are the marginal density distribution functions.

The unbiased and normalized cross-correlation function (CCF) is another suitable strategy to verify mode coupling. For projections Q_{s_1} and Q_{s_2}, the cross-correlation expression is

$$r_{s_1s_2}(t) = \frac{\langle Q_{s_1}(t_0)Q_{s_2}(t_0 + t)\rangle_{t_0}}{\langle Q_{s_1}(t_0)Q_{s_2}(t_0)\rangle_{t_0}} \tag{3}$$

which reveals the time-dependent relationship between Q_{s_1} and Q_{s_2}.

2.2. Local Quantum Vibration Embedding (LQVE) Method and Applications

2.2.1. Local Quantum Vibration Embedding. In order to accurately compute vibrational spectra, it is essential to establish a robust statistical mechanics foundation while also ensuring the reliability of the potential energy surface (PES) and dipole moment surface (DMS). However, for complex systems such as β-HMX, constructing a global PES or DMS is often impractical. Furthermore, molecular mechanics (MM) force fields frequently fall short of the precision required for spectroscopy.[36,37] Therefore, it becomes imperative to consider QM methods for on-the-fly calculations of the potential energy and dipole moments, which are computationally expensive. The LQVE method we propose is to solve the dilemma and obtain the instantaneous vibrational states.

Compared to analytic forms of PES, the discrete variable representation (DVR) offers a more cost-effective solution, where localized functions, i.e., the DVR grids, are used as the basis for solving the vibrational Schrödinger equation, and potential energy provided by electronic structure theory is diagonal in DVR. Notably, the potential optimized DVR (PODVR)[38] allows customization to the specific molecules under investigation, thereby achieving a better balance between computational cost and accuracy. Adding the PODVR grids $\boldsymbol{Q}_{s,i}$ ($i = 1, ..., N^{PO}$) to the coordinates of the probe molecule, the N^{PO} copies $\boldsymbol{x}_n(t;\boldsymbol{Q}_{s1},\boldsymbol{Q}_{s2})$ and potential energy at a given moment in the trajectory can be derived. PODVR is applied to the vicinity of the reference structure, i.e., $\boldsymbol{r}_e$, to get $\hat{H}^{ref}$ and $\boldsymbol{Q}_{s,i}$.

The projection of Cartesian coordinates into vibrational modes can be referenced in a previous subsection. Then, we embed the quantum vibrational modes ξ_{s_1} and ξ_{s_2} of the probe molecules into the MD trajectory while keeping the rest unchanged to get the time-dependent local vibrational Hamiltonian. For the ith PODVR grid, its coordinates are replaced as

$$\tilde{\boldsymbol{x}}_i \leftarrow (\mathbf{U}\cdot(\tilde{\boldsymbol{x}} + \tilde{Q}_{s_1,i}\tilde{\boldsymbol{\xi}}_{s_1} + \tilde{Q}_{s_2,i}\tilde{\boldsymbol{\xi}}_{s_2})) + \tilde{\boldsymbol{t}} \tag{4}$$

in which the symbols with a tilde (∼) represent the mass-weighted one.

The potential energy difference between vibration-embedded structure V and reference structure V^{ref} may be considered as the perturbation V^{per}. Thus, we construct the effective Hamiltonian on PODVR as

$$\begin{aligned}\hat{H}^{eff} &= \hat{H}^{ref} + \hat{H}^{per} \\ &= \sum_{ij} H_{ij}^{ref}|i\rangle\langle j| + \sum_{ij}(V - V^{ref})|i\rangle\langle \quad j|\cdot\delta_{ij} \\ &= \sum_{ij} H_{ij}^{ref}|i\rangle\langle j| + \sum_{i} V^{per}(\boldsymbol{Q}_{s,i})|i\rangle\langle i|.\end{aligned} \tag{5}$$

where H_{ij}^{ref} and $|i\rangle$ are Hamiltonian matrix elements of the reference structure and the localized basis, i.e., PODVR grids, respectively. Instantaneous physical quantities, such as instantaneous frequency, dipole, polarizability, etc., can be computed based on the Hamiltonian.

2.2.2. State Population Relaxation. To obtain the state population relaxation from one vibrational state to others,[39,40] the time-dependent Schrödinger equation is written as

$$i\hbar\frac{\partial}{\partial t}|\psi\rangle = \hat{H}^{eff}|\psi\rangle \tag{6}$$

in which the $\hat{H}^{eff}$ is calculated by the LQVE method. Energy transfer pathways between coupled modes and their time scales can be determined by solving the time-dependent Schrödinger equation, which, for such small Hamiltonian matrices, can be solved by first getting the eigenstates of the Hamiltonian and then integrating over time on the stationary states, where only phases are altered. Note that the time of the quantum-state evolution here is not equivalent to the time in the classical dynamical trajectory.

2.2.3. Third-Order Response Functions of the Two-Dimensional Infrared (2D IR) Spectroscopy. Ultrafast 2D IR spectroscopy is commonly used to comprehend the forces of coupling modes in molecules. The forces are indirectly manifested through the vibrational levels and hence manage the IVR process.[41] The cross peaks of 2D-IR spectroscopy can demonstrate the coupling of different quantum states in the system effectively,[42] making it beneficial for usage in energetic materials.

The 2D-IR spectra can be achieved by the Fourier transformation of the total response functions[43]

$$R = R_r + R_{nr} = \sum_{i=1}^{6} R_i(t_1, t_2, t_3) \tag{7}$$

where R_r and R_{nr} represent the rephasing and nonrephasing responses, respectively. Considering semiclassical treatment and the Condon approximation

https://doi.org/10.1021/jacsau.4c00775
JACS Au 2024, 4, 4455−4465

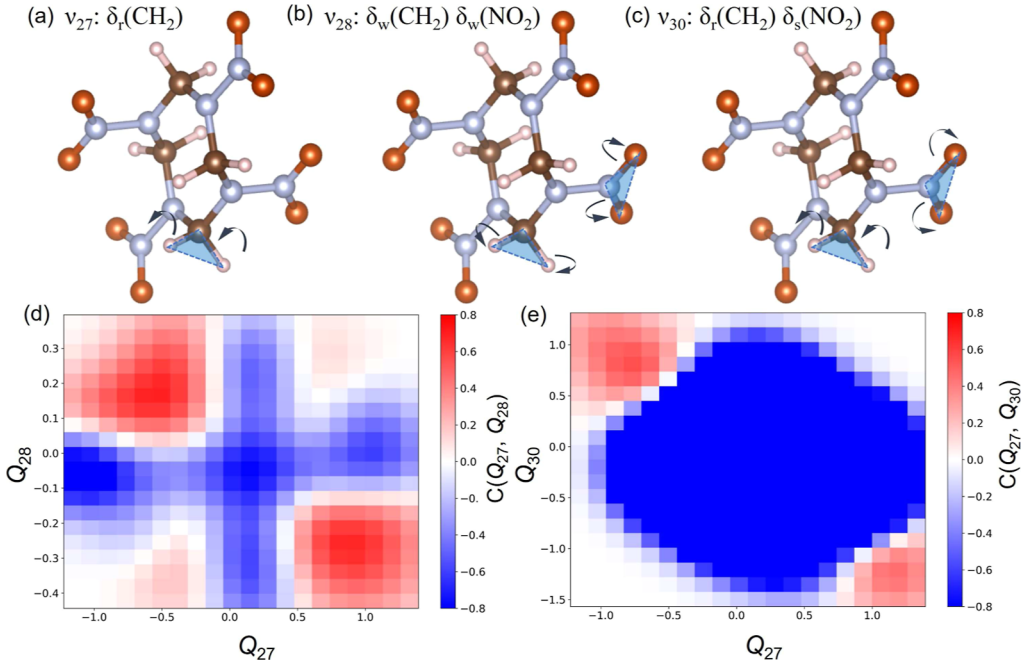

Figure 2. (a) ν_{27}, ~417 cm^{-1}, rocking in the CH_2 plane; (b) ν_{28}, ~575 cm^{-1}, wagging of two H atoms out of the CH_2 plane and two O atoms out of the NO_2 plane; (c) ν_{30}, ~605 cm^{-1}, rocking in the CH_2 plane and scissoring in the NO_2 plane; (d) CDF plots between ν_{27} and ν_{28}; (e) CDF plots between ν_{27} and ν_{30}. When Q_i and Q_j are completely uncorrelated, i.e., the 2D histogram is equal to the direct product of two 1D histograms, $C(Q_i, Q_j)$ is zero. When the combined density distribution of Q_i and Q_j exceeds that of the individual, the plot shows a positive correlation in red. Blue represents a negative association.

$$
\begin{aligned}
R_1(t_1, t_2, t_3) &= R_2(t_1, t_2, t_3) \\
&= \langle |\mu_{10}|^4 e^{i\int_0^{t_1} d\tau\, \omega_{10}(\tau) - i\int_{t_1+t_2}^{t_1+t_2+t_3} d\tau\, \omega_{10}(\tau)} \rangle \\
&\quad \Gamma_1(t_3, t_2, t_1), \\
R_4(t_1, t_2, t_3) &= R_5(t_1, t_2, t_3) \\
&= \langle |\mu_{10}|^4 e^{-i\int_0^{t_1} d\tau\, \omega_{10}(\tau) - i\int_{t_1+t_2}^{t_1+t_2+t_3} d\tau\, \omega_{10}(\tau)} \rangle \\
&\quad \Gamma_1(t_3, t_2, t_1), \\
R_3(t_1, t_2, t_3) &= -\langle |\mu_{10}|^2 |\mu_{21}|^2 \\
&\quad e^{i\int_0^{t_1} d\tau\, \omega_{10}(\tau) - i\int_{t_1+t_2}^{t_1+t_2+t_3} d\tau\, \omega_{21}(\tau)} \rangle \Gamma_2(t_3, t_2, t_1), \\
R_6(t_1, t_2, t_3) &= -\langle |\mu_{10}|^2 |\mu_{21}|^2 \\
&\quad e^{-i\int_0^{t_1} d\tau\, \omega_{10}(\tau) - i\int_{t_1+t_2}^{t_1+t_2+t_3} d\tau\, \omega_{21}(\tau)} \rangle \Gamma_2 \\
&\quad (t_3, t_2, t_1),
\end{aligned} \tag{8}
$$

where μ_{ij} and ω_{ij} denote the instantaneous transition dipole moment and frequency between ith and jth energy levels, respectively. $\langle \cdots \rangle$ denotes the classical ensemble average. t_i (i = 1, 2, and 3) represents the corresponding time gap between different lights, where t_2 is typically set as the waiting time. Γ_1 and Γ_2 denote lifetime-broadening factors that phenomenally describe the population relaxation.[44] Instantaneous vibrational frequencies can be calculated by diagonalizing eq S, and the transition dipole moments can then be calculated with the corresponding wave functions.

2.3. Computational and Experimental Details

The β-HMX single crystal with the $P2_1/n$ space group is enlarged into a 2 × 2 × 2 supercell using the VESTA[45] and Atomsk[46] packages to enhance the realism of environmental influences. The ASE package[47] is utilized to determine the equilibrium structures and Hessian matrix. The MD trajectories are carried out with the LAMMPS[48] package, employing a force field built by machine learning (see Supporting Information for details).

All vibrational modes are projected using our in-house vibrational projection program after importing the MD trajectory, equilibrium molecular structure, and vibrational modes. The trajectories are analyzed using the MDAnalysis software.[49] Utilizing the LQVE method, potential energy and instantaneous frequencies of the supercell at specific frames are calculated in the GFN2-xTB level,[50] where the probe molecules have been replaced by the molecular structures generated by the N^{PO} grids. The state population relaxation time evolution as well as 2D IR spectra are computed by our in-house code.[51,52]

A solid, polycrystalline β-HMX film is produced by physical vapor deposition onto a diamond substrate, yielding the 1 μm thick sample used herein. The vibrational dynamics of the β-HMX film were measured in real-time using ultrafast far-infrared transient absorption spectroscopy (TAS), and the experimental details have been previously reported.[53,54] The spot sizes of the far-infrared probe beam and mid-infrared pump beam are 0.2 and 0.3 mm, respectively, with pulse widths of the probe and pump beam being 0.1 and 0.2 ps, respectively. The pump fluence is 6 mJ/cm^2, and the instrumental response time is 0.3 ps for all frequencies, with a spectral resolution of 4 cm^{-1}.

https://doi.org/10.1021/jacsau.4c00775
JACS Au 2024, 4, 4455−4465

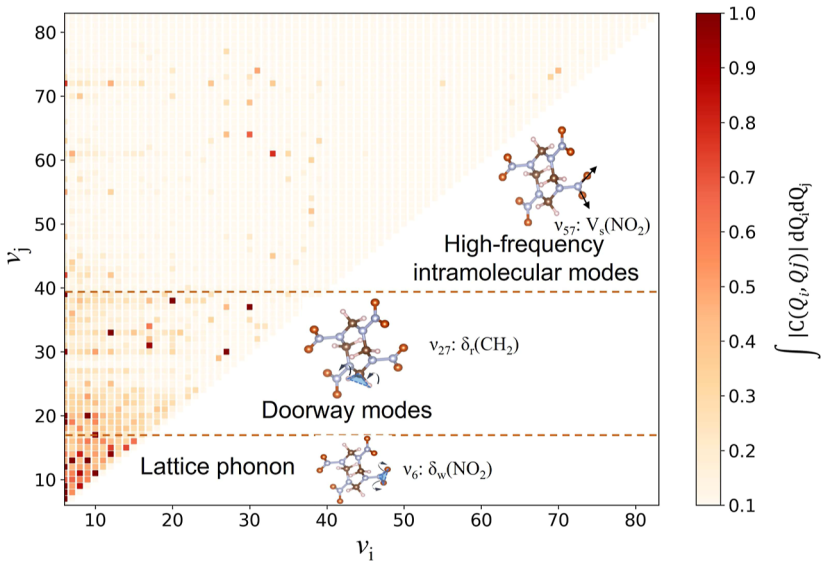

Figure 3. Correlation heat map for ν_i and ν_j.

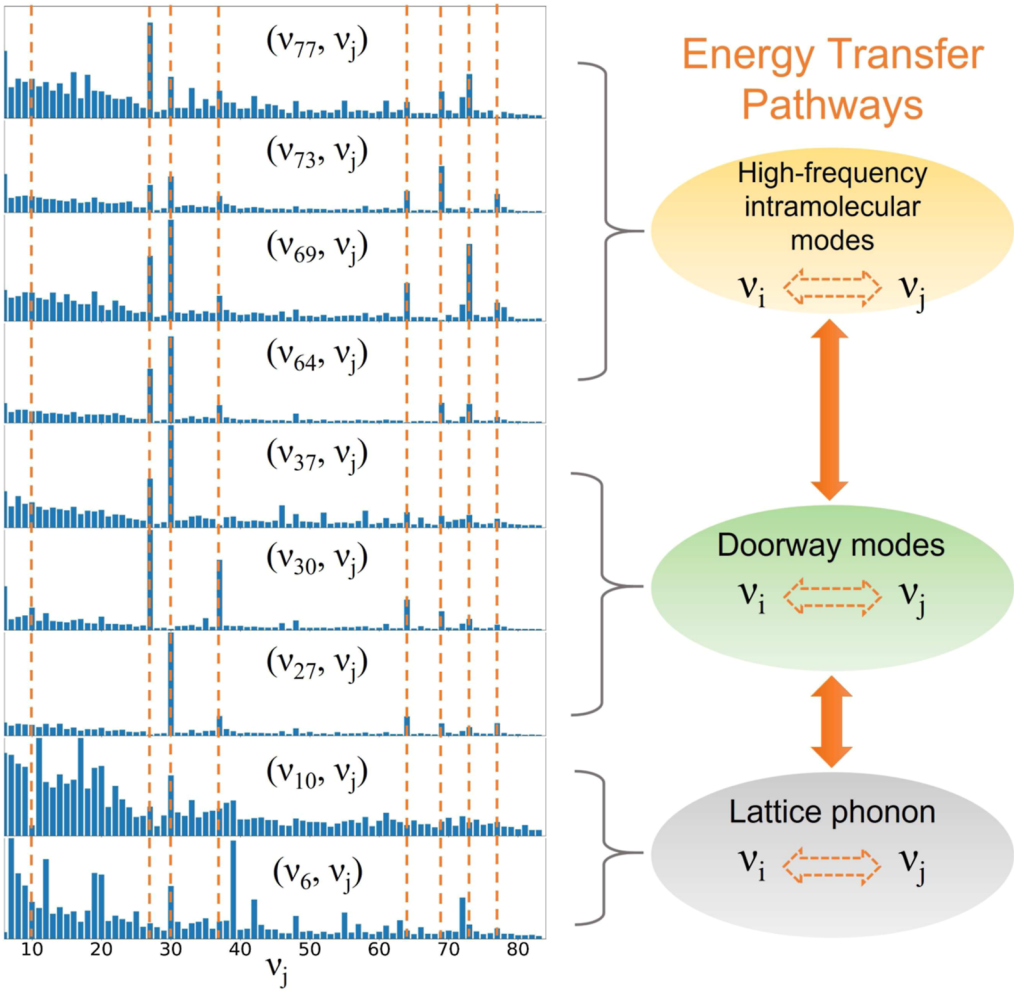

Figure 4. Example of energy transfer pathways. The $\int |C(Q_i, Q_j)| dQ_i dQ_j$ of certain mode with other modes located in different frequency regions indicates a strong correlation between this group of modes.

https://doi.org/10.1021/jacsau.4c00775
JACS Au 2024, 4, 4455−4465

3. RESULTS AND DISCUSSION

3.1. Energy Transfer Pathways for Coupled Modes

The coupling of modes is a prerequisite for the transfer of energy. Figure 2 shows two CDF plots of the vibrational mode ν_{27}, which may be easily explained using eq 2. The correlations demonstrated in Figure 2d,e gradually increase, and it can be seen that there is a strong negative correlation between ν_{27} (~417 cm^{-1}, rocking in the CH_2 plane) and ν_{30} (~605 cm^{-1}, rocking in the CH_2 plane and scissoring in the NO_2 plane), while the correlation between ν_{27} and ν_{28} (~575 cm^{-1}, wagging of two H atoms out of the CH_2 plane and two O atoms out of the NO_2 plane) is relatively weak.

Integrating the absolute values of $C(Q_i, Q_j)$ in each correlation plot identifies strongly coupled vibrational modes. For example, the integral value of ν_{27} and ν_{30} in Figure 2 is 4.75, whereas only 0.04 of ν_{27} and ν_{28}. The heat map in Figure 3 shows that the coupling between the low-frequency modes (lattice phonon, LP) is greater than the coupling between the low-frequency and middle-frequency modes (doorway mode, located approximately in the 200−750 cm^{-1} range,[13,55] DM), and the coupling between the high-frequency intramolecular modes (HIM) is much smaller than the first two.

Analyzing $\int |C(Q_i, Q_j)| dQ_i dQ_j$ for all combined modes reveals groups of tightly coupled modes. For example, as the integral value bar shown in Figure 4, ν_6, ν_{10}, and ν_{27} are all strongly coupled with ν_{30} correspondingly, whereas ν_{27} and ν_{30} are strongly coupled with ν_{37}, ν_{64}, ν_{69}, ν_{73}, and ν_{77}. This indicates that when energy is transferred from the intermolecular to the lattice phonons ν_6 and ν_{10} and the doorway mode ν_{27}, they are more likely to transfer excess energy to mode ν_{30} than to other modes. The doorway modes ν_{27}, ν_{30}, and ν_{37} further transfer excess energy to the high-frequency intramolecular mode. The high-frequency intramolecular modes may transfer excess energy to each other, but this is far less common. In this energy transfer pathway, excess energy is gathered on mode ν_{77}, which is associated with the symmetric stretch of CH_2 and in good agreement with the recent theoretical findings.[24] When ν_{77} is excited, energy tends to relax along the energy transfer pathway. As the name suggests, the doorway modes adequately characterize its function, especially those of ν_{27} and ν_{30}.

Similar pathways may also exist in groups ν_6, ν_9, ν_{20}, ν_{38}, ν_{50}, ν_{52}, ν_{54}, and ν_{60} as well as groups ν_{12}, ν_{33}, ν_{42}, ν_{45}, ν_{55}, ν_{61}, ν_{72}, etc.; detailed data is available in Supporting Information. In conclusion, when lattice phonons of β-HMX crystal molecules are pumped, energy tends to pass between lattice phonons to each other, followed by a transfer from the doorway modes to the high-frequency modes. The probability of energy transfer between most of the high-frequency modes is minimal. Similarly, as high-frequency modes are pumped, the relaxation process tends to transfer excess energy to lower frequencies via such energy transfer pathways. The phenomenon is in good agreement with the recent research.[15]

CDF analysis is based on the cumulative of the entire MD trajectory and does not have time-dependent properties. On the contrary, the cross-correlation function can reflect the relationship between two variables across time. Figure 5 illustrates a portion of the cross-correlation function over time, with modes selected from the example of the energy transfer pathways discussed above. The evolution of the cross-correlation functions over time for these coupled modes tends to be rather consistent, notably for (ν_{27}, ν_{30}), (ν_{27}, ν_{37}), and (ν_{30}, ν_{37}). This finding supports the previous conclusions and suggests that the coupled modes exhibit correlation not only statistically but also dynamically.

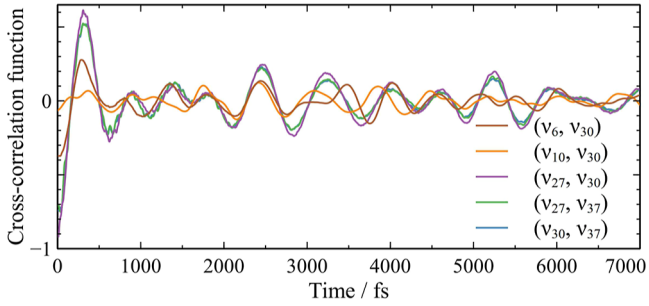

Figure 5. Cross-correlation function between parts of vibrational modes.

3.2. State Population Relaxation and 2D IR Spectra

The preceding analysis has provided valuable information about mode coupling; nevertheless, it is not appropriate for investigating more subtle mechanisms. Meanwhile, experimental observation of transition frequencies is available, but resolving time-dependent wave function evolution is difficult. As a result, we further investigated mode coupling based on the time-dependent Schrödinger equation. By constructing the effective Hamiltonian quantities shown in eq 5 and performing the state population relaxation time evolution, information about the energy transfer between different vibrational states of coupled modes can be obtained.

Based on the above statistical analysis, we chose to explore the strongly coupled DM−DM ν_{27} and ν_{30}, as well as LP-DM ν_{10} and ν_{30} as examples. Figure 6 shows the ensemble-averaged energy transfer process of (ν_{27}, ν_{30}) and (ν_{10}, ν_{30}) with the initial states $|10\rangle$ or $|01\rangle$, respectively. For ν_{27} and ν_{30}, when the pump pulse excites state $|10\rangle$ (Figure 6 (a)), the probability of energy transfer to each final state is $|01\rangle$, $|20\rangle$, $|00\rangle$, and $|11\rangle$. The order of exciting state $|01\rangle$ (Figure 6 (b)) is $|10\rangle$, $|02\rangle$, $|11\rangle$, and $|00\rangle$. For excited $|10\rangle$, whether the energy transfers to $|20\rangle$ or to $|00\rangle$, both reflect the anharmonic vibration of ν_{27}. However, the energy transfer to $|01\rangle$ and the combination state $|11\rangle$ provide significant evidence for the coupling of ν_{27} and ν_{30}.

Similarly, assuming $|01\rangle$ as the initial state, energy transfer to $|10\rangle$ and $|11\rangle$ demonstrates the strong coupling between ν_{27} and ν_{30}. By ensemble averaging the instantaneous frequencies calculated by the LQVE method, the ultrafast energy transfer process was found to equilibrate at 800 fs when the excited state is $|10\rangle$ and 1500 fs when the excited state is $|01\rangle$. ν_{10} and ν_{30} have a substantially higher energy transfer ratio than those of ν_{27} and ν_{30}. When $|10\rangle$ is excited, the probability of transferring energy to the combination state is negligible, but when the $|01\rangle$ state is excited, a significant fraction of energy relaxed to the combination state. Both energy transfer processes take about 700 fs.

The ~1280 cm^{-1} of the HMX molecule is of great interest as it is related to the symmetric stretching of NO_2.[54,56] The experimental transient absorption spectra in Figure 7a,b indicate that when ~1280 cm^{-1} is pumped at 3.1 ps, its absorption signal decreases consistently over time. After an ultrafast period of around 400 fs, stronger absorption signals are probed at ~730 and ~760 cm^{-1}, which also begin to decrease after passing through 750 fs to 1.2 ps. The consistent trend in Figure 7a,b implies a strong correlation between ~730 cm^{-1}/~ 760 cm^{-1} and ~1280 cm^{-1}, and the two time periods may be the energy

https://doi.org/10.1021/jacsau.4c00775
JACS Au 2024, 4, 4455−4465

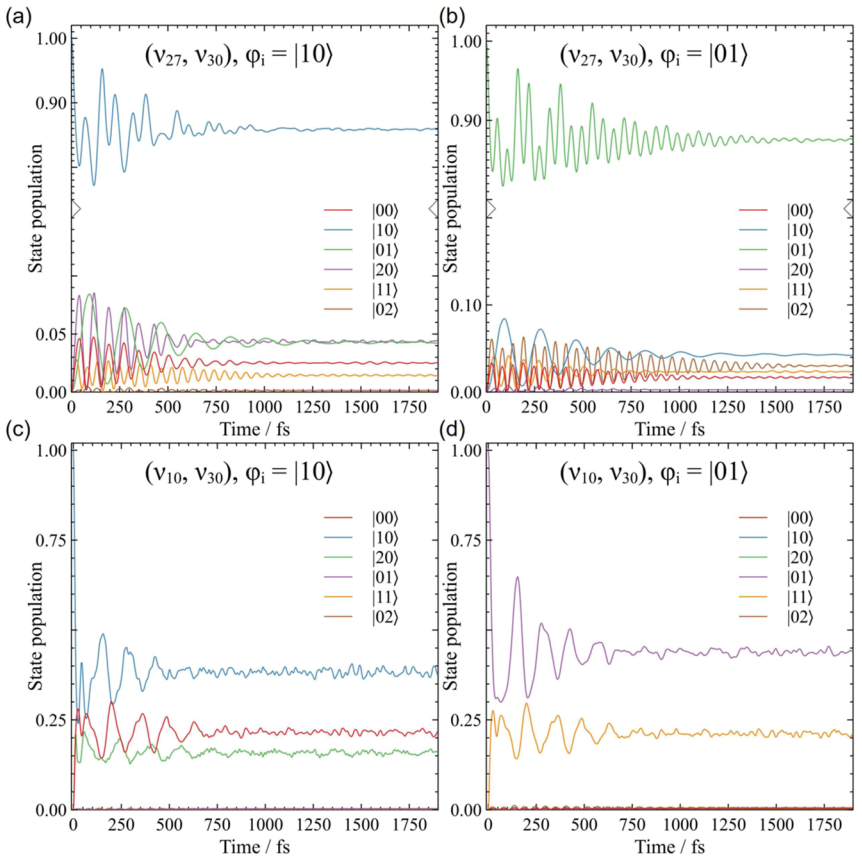

Figure 6. State population relaxation time evolution of (a) (ν_{27}, ν_{30}) with |10⟩ as the initial state, (b) (ν_{27}, ν_{30}) with |01⟩ as the initial state, (c) (ν_{10}, ν_{30}) with |10⟩ as the initial state, and (d) (ν_{10}, ν_{30}) with |01⟩ as the initial state.

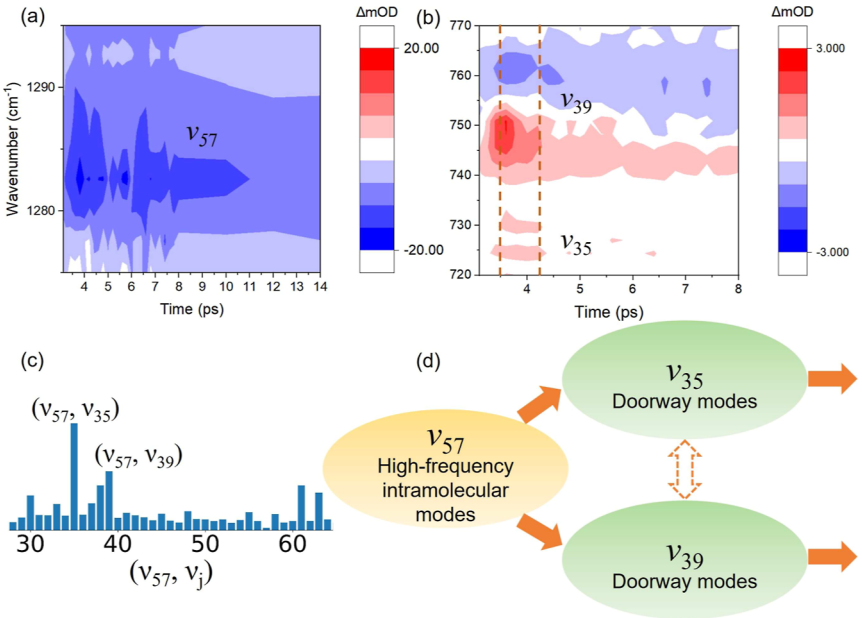

Figure 7. (a,b) Transient absorption spectra from the experiment (start time t_0 = 3.1 ps; ΔmOD means variation of the optical density). (c) Integral value bar for ν_{57}. (d) Possible energy transfer pathways.

relaxation times. To answer this question more deeply, we chose three corresponding doorway modes: ν_{35}, ν_{39}, and high-frequency intramolecular mode ν_{57}, for the quantum mechanical study. The statistical analysis of Figure 7c confirmed a strong coupling between the three modes. Thus, we hypothesize the energy relaxation process in Figure 7d, where the excess energy is first transferred from ν_{57} to ν_{35} and ν_{39}, respectively; both processes are about 400 fs, and after the energy reaches ν_{35} and ν_{39}, it is further transferred to each other or to lower frequencies, and this process takes about 700 fs to 1.2 ps.

To test the above conjecture, we performed an analysis of the state-population relaxation time evolution. The state population

https://doi.org/10.1021/jacsau.4c00775
JACS Au 2024, 4, 4455−4465

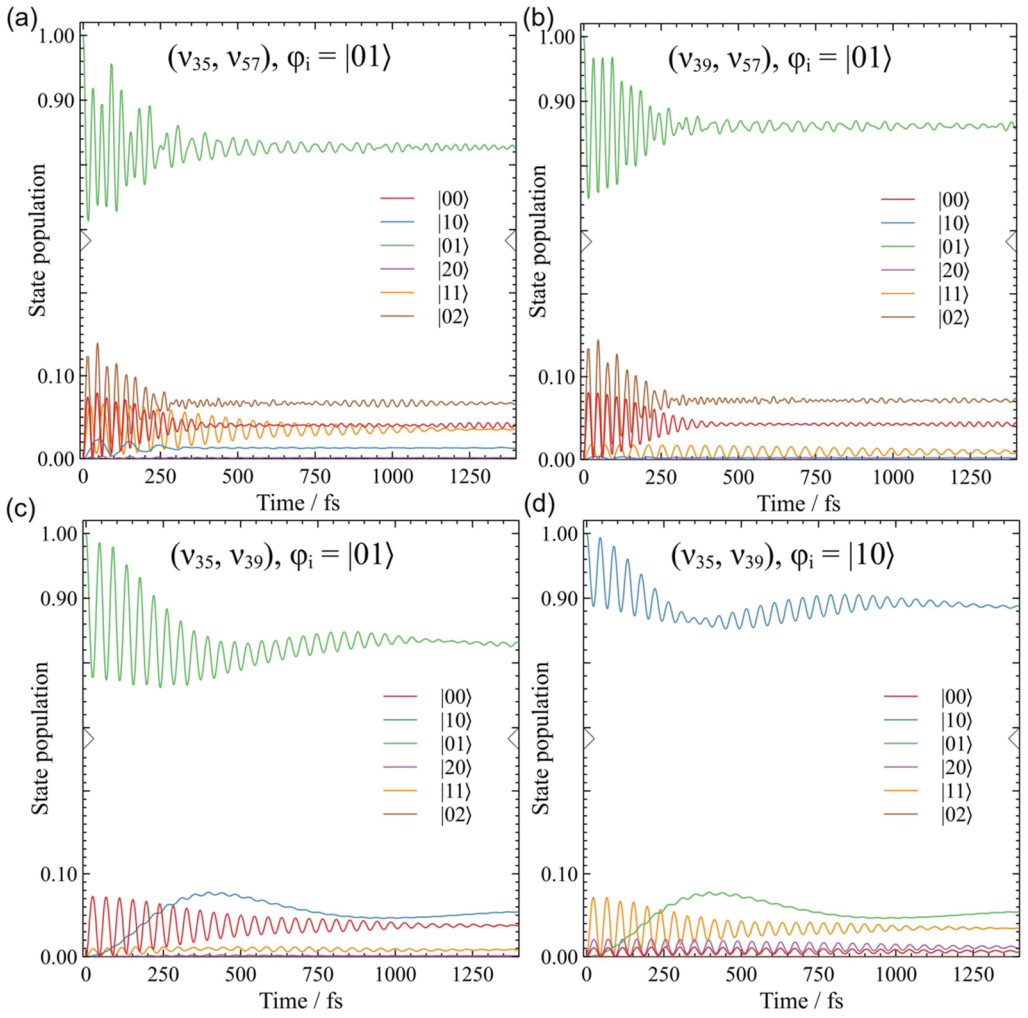

Figure 8. State population relaxation time evolution of (a) (ν_{35}, ν_{57}) with $|01\rangle$ as the initial state, (b) (ν_{39}, ν_{57}) with $|01\rangle$ as the initial state, (c) (ν_{35}, ν_{39}) with $|01\rangle$ as the initial state, and (d) (ν_{35}, ν_{39}) with $|10\rangle$ as the initial state.

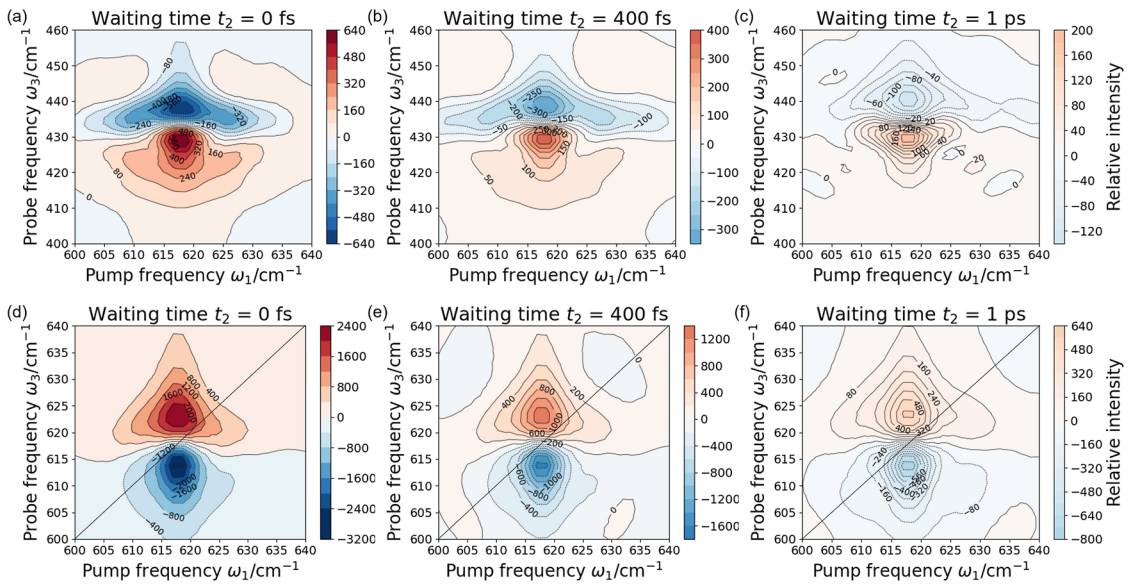

Figure 9. (a–c) Cross-peaks of the 2D IR spectra of modes ν_{27} and ν_{30} with the higher oscillator excited at the waiting time t_2 equaling 0 fs, 400 fs, and 1 ps, respectively. (d–f) Diagonal peaks of the 2D IR spectra of modes ν_{27} and ν_{30} at the waiting time t_2 equaling 0 fs, 400 fs, and 1 ps, respectively.

relaxation time evolution, as shown in Figure 8, indicated the coupling and energy transfer between DM-HIM ν_{35} and ν_{57}, DM-HIM ν_{39} and ν_{57}, and DM–DM ν_{35} and ν_{39}, and the calculated relaxation times are about 400, 350, and 800 fs,

https://doi.org/10.1021/jacsau.4c00775
JACS Au 2024, 4, 4455–4465

respectively. At the quantum-state level, it can be observed that after the excitation of ν_{57} ($|01\rangle$), the relaxation to the state $|10\rangle$ and the combination state $|11\rangle$ of ν_{39} and ν_{57} does not have much energy, which suggests that energy transfer between ν_{39} and ν_{57} is not as easy as that between ν_{35} and ν_{57}. However, statistical analysis shows a strong correlation between ν_{39} and ν_{57}. This confusion can be clarified by Figure 8c,d. When doorway mode ν_{35} or ν_{39} is excited, the energy mainly relaxes to the first excited state of the other mode. Specifically, when ν_{35} is excited, the energy relaxing to the combination state $|11\rangle$ also accounts for a considerable proportion. This suggests the strong coupling between ν_{35} and ν_{39}, and the energy prefers relaxing from ν_{57} to ν_{35} and then transfers from ν_{35} to ν_{39}, which can also be confirmed in Figure 7b, where the experimental signal of 730 cm^{-1} no longer exists after 750 fs, and our calculated relaxation time between ν_{35} and ν_{39} reaches equilibrium at 800 fs. The time scale is also compatible with the previous study of the NO_2 vibrations of HMX in solution[23] or other energetic materials[22] on the time scale of 1 ps.

The 2D IR spectra can provide a direct measure of the anharmonicity of the probe mode. Experimentalists characterize the IVR process between coupled modes by the decreasing intensities of the peaks of the 2D IR spectra.[23] In our work, we obtain the time of the IVR process between the coupled modes through the time evolution of the state population relaxation described above, which may therefore affect the decreasing intensities of the peaks in the calculated 2D IR spectra.

Off-diagonal anharmonicity makes cross-peaks appear. It is a direct manifestation of coupling between two vibrational modes, which means that the transition frequency of one mode depends on the excitation level of the other mode. It is also in good agreement with the conclusions on the coupling of the two models in Figure 6. The blue shift in the spectrum is due to the considerable fourth-order force constant of the potential energy surface. In Figure 9a−c, cross-peaks of the 2D IR spectra of ν_{27} and ν_{30} with the higher oscillator excited at the waiting time t_2 equaling 0 fs, 400 fs, and 1 ps are presented. The negative (blue) peak comes from the $|01\rangle \rightarrow |11\rangle$ transition. The line shape changes significantly with time, and the center frequency is blue-shifted during the process. The variation of the line shape reaches equilibrium at 800 fs to 1 ps. In contrast, the positive (red) peak representing the $|00\rangle \rightarrow |10\rangle$ transition does not vary significantly as a function of the waiting time, which is well consistent with the experimental observations of HMX in solution.[23] One of the reasons for this is that the $|10\rangle$ state is more stable than the $|11\rangle$ state. The red and blue peaks in Figure 9d−f reflect the anharmonic frequency shifts of ν_{30}. The line shape changes insignificantly with time, which may also be a reason for the phenomenon in the cross-peaks.

4. CONCLUSIONS

In this work, for the first time, we use a combination of vibrational projection, statistical analysis, and local quantum vibrational embedding to demonstrate the intramolecular vibrational energy transfer process of typical explosives, β-HMX. This provides a powerful reference and innovative program for the study of condensed materials. We respond to the controversial question about doorway modes in energy transfer pathways at the level of quantum mechanics, and our findings indicate that doorway modes serve as vital mediators.

We develop a combined distribution function method based on the vibrational mode coordinate to improve its application to condensed matter systems. The statistical analysis results indicated the energy transfer pathways that when the β-HMX crystal is shocked, excess energy tends to be rapidly distributed in the low-frequency modes, transfers through the doorway modes to the high-frequency intramolecular modes, and the possibility of transfer between most of the high-frequency modes being extremely unlikely. State population relaxation time evolution confirms the process at the quantum-state level, explains microscopic details that cannot be explained by statistical analysis, and determines the time scale at fs. In turn, the relaxation process that occurs when high-frequency modes are pumped and transfer excess energy into lower frequencies tends to follow such an energy transfer pathway. We also perform state population relaxation calculations and have experimental spectra to validate our findings. Our conclusion is in good agreement with the experimental and theoretical studies reported. The 2D-IR spectra are computed to investigate the vibrational energy transfer process of HMX theoretically; the nondiagonal cross-peaks provide important evidence of the mode coupling. Time scales of energy transfer and change trends of the linear shape are consistent with those of the relevant experiment.

Through detailed analysis and theoretical exploration, this study reveals the complex dynamical process of intramolecular vibrational energy transfer in the β-HMX, which can be flexibly generalized to study other explosive materials, thereby contributing to the advancement of both fundamental scientific knowledge and practical applications in the field of explosives research.

■ ASSOCIATED CONTENT

Supporting Information

The Supporting Information is available free of charge at https://pubs.acs.org/doi/10.1021/jacsau.4c00775.

Raw data of molecular dynamics simulation, vibrational projection, and the LQVE method (ZIP)

■ AUTHOR INFORMATION

Corresponding Authors

Huajie Song − *Institute of Applied Physics and Computational Mathematics, Beijing 100088, China*; Email: song_huajie@iapcm.ac.cn

Yanqiang Yang − *National Key Laboratory of Shock Wave and Detonation Physics, Institute of Fluid Physics, China Academy of Engineering Physics, Mianyang 621900, China*; orcid.org/0000-0003-2184-8126; Email: yqyang@caep.cn

Hui Li − *Institute of Theoretical Chemistry, College of Chemistry, Jilin University, Changchun 130023, China*; orcid.org/0000-0002-2689-2241; Email: prof_huili@jlu.edu.cn

Authors

Jia Liu − *Institute of Theoretical Chemistry, College of Chemistry, Jilin University, Changchun 130023, China*; orcid.org/0000-0002-1183-6474

Jitai Yang − *Institute of Theoretical Chemistry, College of Chemistry, Jilin University, Changchun 130023, China*; orcid.org/0000-0003-1172-0401

Gangbei Zhu − *National Key Laboratory of Shock Wave and Detonation Physics, Institute of Fluid Physics, China Academy of Engineering Physics, Mianyang 621900, China*

https://doi.org/10.1021/jacsau.4c00775
JACS Au 2024, 4, 4455−4465

Jiarui Li − *Institute of Theoretical Chemistry, College of Chemistry, Jilin University, Changchun 130023, China*
You Li − *Institute of Theoretical Chemistry, College of Chemistry, Jilin University, Changchun 130023, China;* orcid.org/0000-0003-4882-8459
Yu Zhai − *Beijing National Laboratory for Molecular Sciences, Institute of Theoretical and Computational Chemistry, College of Chemistry and Molecular Engineering, Peking University, Beijing 100871, China;* orcid.org/0000-0002-5065-688X

Complete contact information is available at: https://pubs.acs.org/10.1021/jacsau.4c00775

Author Contributions

CRediT: **Jia Liu** conceptualization, data curation, formal analysis, investigation, methodology, software, visualization, writing - original draft; **Jitai Yang** methodology, software, writing - review & editing; **Gangbei Zhu** data curation, validation, writing - review & editing; **Jiarui Li** software, writing - review & editing; **You Li** methodology, software, writing - review & editing; **Yu Zhai** methodology, software, writing - review & editing; **Huajie Song** data curation, project administration, resources; **Yanqiang Yang** project administration, resources; **Hui Li** conceptualization, project administration, resources, supervision, writing - review & editing.

Notes

The authors declare no competing financial interest.

■ ACKNOWLEDGMENTS

The author thanks the support from the 2020-JCJQ project (GFJQ2126-007), as well as the help from Ke Li on this work.

■ REFERENCES

(1) Xiang, B.; Ribeiro, R. F.; Du, M.; Chen, L.; Yang, Z.; Wang, J.; Yuen-Zhou, J.; Xiong, W. Intermolecular vibrational energy transfer enabled by microcavity strong light−matter coupling. *Science* **2020**, *368*, 665−667.
(2) Uzer, T.; Miller, W. Theories of intramolecular vibrational energy transfer. *Phys. Rep.* **1991**, *199*, 73−146.
(3) Owrutsky, J. C.; Raftery, D.; Hochstrasser, R. M. Vibrational Relaxation Dynamics in Solutions. *Annu. Rev. Phys. Chem.* **1994**, *45*, 519−555.
(4) Yu, Q.; Bowman, J. M. Manipulating hydrogen bond dissociation rates and mechanisms in water dimer through vibrational strong coupling. *Nat. Commun.* **2023**, *14*, 3527.
(5) Wilcken, R.; Nishida, J.; Triana, J. F.; John-Herpin, A.; Altug, H.; Sharma, S.; Herrera, F.; Raschke, M. B. Antenna-coupled infrared nanospectroscopy of intramolecular vibrational interaction. *Proc. Natl. Acad. Sci. U.S.A.* **2023**, *120*, No. e2220852120.
(6) Chen, T.-T.; Du, M.; Yang, Z.; Yuen-Zhou, J.; Xiong, W. Cavity-enabled enhancement of ultrafast intramolecular vibrational redistribution over pseudorotation. *Science* **2022**, *378*, 790−794.
(7) Wang, D. S.; Neuman, T.; Yelin, S. F.; Flick, J. Cavity-Modified Unimolecular Dissociation Reactions via Intramolecular Vibrational Energy Redistribution. *J. Phys. Chem. Lett.* **2022**, *13*, 3317−3324.
(8) Thomas, A.; Lethuillier-Karl, L.; Nagarajan, K.; Vergauwe, R. M. A.; George, J.; Chervy, T.; Shalabney, A.; Devaux, E.; Genet, C.; Moran, J.; Ebbesen, T. W. Tilting a ground-state reactivity landscape by vibrational strong coupling. *Science* **2019**, *363*, 615−619.
(9) Grubb, M. P.; Coulter, P. M.; Marroux, H. J. B.; Orr-Ewing, A. J.; Ashfold, M. N. R. Unravelling the mechanisms of vibrational relaxation in solution. *Chem. Sci.* **2017**, *8*, 3062−3069.
(10) Zeman, S.; Jungová, M. Sensitivity and Performance of Energetic Materials. *Propellants, Explos., Pyrotech.* **2016**, *41*, 426−451.
(11) Joshi, K.; Losada, M.; Chaudhuri, S. Intermolecular Energy Transfer Dynamics at a Hot-Spot Interface in RDX Crystals. *J. Phys. Chem. A* **2016**, *120*, 477−489.
(12) Tokmakoff, A.; Fayer, M. D.; Dlott, D. D. Chemical reaction initiation and hot-spot formation in shocked energetic molecular materials. *J. Phys. Chem.* **1993**, *97*, 1901−1913.
(13) Michalchuk, A. A. L.; Hemingway, J.; Morrison, C. A. Predicting the impact sensitivities of energetic materials through zone-center phonon up-pumping. *J. Chem. Phys.* **2021**, *154*, 064105.
(14) Aubuchon, C.; Rector, K.; Holmes, W.; Fayer, M. Nitro group asymmetric stretching mode lifetimes of molecules used in energetic materials. *Chem. Phys. Lett.* **1999**, *299*, 84−90.
(15) Kumar, G.; VanGessel, F. G.; Munday, L. B.; Chung, P. W. 3-Phonon Scattering Pathways for Vibrational Energy Transfer in Crystalline RDX. *J. Phys. Chem. A* **2021**, *125*, 7723−7734.
(16) Bondarchuk, S. V. Theory of impact sensitivity revisited: mechanical-to-vibrational energy transfer phenomenon. *FirePhysChem.* **2022**, *2*, 334−339. Progress in Solid Rocket Propulsion - Part B
(17) Kraczek, B.; Chung, P. W. Investigation of direct and indirect phonon-mediated bond excitation in α-RDX. *J. Chem. Phys.* **2013**, *138*, 074505.
(18) Cole-Filipiak, N. C.; Knepper, R.; Wood, M.; Ramasesha, K. Mode-Selective Vibrational Energy Transfer Dynamics in 1,3,5-Trinitroperhydro-1,3,5-triazine (RDX) Thin Films. *J. Phys. Chem. A* **2021**, *125*, 7788−7802.
(19) Cole-Filipiak, N. C.; Marquez, M.; Knepper, R.; Harmon, R.; Wiese-Smith, D.; Schrader, P.; Wood, M.; Ramasesha, K. Ultrafast spectroscopic studies of vibrational energy transfer in energetic materials. *AIP Conf. Proc.* **2020**, *2272*, 060006.
(20) Ramasesha, K.; Wood, M.; Cole-Filipiak, N. C.; Knepper, R. *Experimental and Theoretical Studies of Ultrafast Vibrational Energy Transfer Dynamics in Energetic Materials*, 2020.
(21) Ostrander, J. S.; Knepper, R.; Tappan, A. S.; Kay, J. J.; Zanni, M. T.; Farrow, D. A. Energy Transfer Between Coherently Delocalized States in Thin Films of the Explosive Pentaerythritol Tetranitrate (PETN) Revealed by Two-Dimensional Infrared Spectroscopy. *J. Phys. Chem. B* **2017**, *121*, 1352−1361.
(22) Shi, L.; Yu, P.; Zhao, J.; Wang, J. Ultrafast Intermolecular Vibrational Energy Transfer in Hexahydro-1,3,5-trinitro-1,3,5-triazine in Molecular Crystal by 2D IR Spectroscopy. *J. Phys. Chem. C* **2020**, *124*, 2388−2398.
(23) Yang, F.; Shi, L.; Dong, T.; Yu, P.; Hu, R.; Wu, H.; Yang, Y.; Wang, J. Solution structures and ultrafast vibrational energy dissipation dynamics in cyclotetramethylene tetranitramine. *J. Chem. Phys.* **2022**, *156*, 194305.
(24) Zhang, L.; Song, H.; Yang, Y.; Zhou, Z.; Zhang, J.; Qu, Z. Ultrafast vibrational energy redistribution in cyclotrimethylene trinitramine (RDX). *J. Chem. Phys.* **2024**, *160*, 064105.
(25) Hooper, J. Vibrational energy transfer in shocked molecular crystals. *J. Chem. Phys.* **2010**, *132*, 014507.
(26) Xue, R.-J.; Grofe, A.; Yin, H.; Qu, Z.; Gao, J.; Li, H. Perturbation Approach for Computing Infrared Spectra of the Local Mode of Probe Molecules. *J. Chem. Theory Comput.* **2017**, *13*, 191−201.
(27) Cong, Y.; Zhai, Y.; Yang, J.; Grofe, A.; Gao, J.; Li, H. Quantum vibration perturbation approach with polyatomic probe in simulating infrared spectra. *Phys. Chem. Chem. Phys.* **2022**, *24*, 1174−1182.
(28) Li, H.; Jensen, J. H. Partial Hessian vibrational analysis: the localization of the molecular vibrational energy and entropy. *Theor. Chem. Acc.* **2002**, *107*, 211−219.
(29) Ghysels, A.; Van Neck, D.; Waroquier, M. Cartesian formulation of the mobile block Hessian approach to vibrational analysis in partially optimized systems. *J. Chem. Phys.* **2007**, *127*, 164108.
(30) Besley, N. A.; Metcalf, K. A. Computation of the amide I band of polypeptides and proteins using a partial Hessian approach. *J. Chem. Phys.* **2007**, *126*, 035101.
(31) Hirano, T.; Taketsugu, T.; Kurita, Y. Vibration Mixing in Terms of Normal Modes. *J. Phys. Chem.* **1994**, *98*, 6936−6941.

(32) Hirano, T.; Taketsugu, T.; Kurita, Y. Vibration Mixing: An Application to the Prediction of the Transition Normal Vibration Mode. *J. Phys. Chem.* **1994**, *98*, 6942−6949.
(33) Kabsch, W. A solution for the best rotation to relate two sets of vectors. *Acta Crystallogr., Sect. A* **1976**, *32*, 922−923.
(34) Kabsch, W. A discussion of the solution for the best rotation to relate two sets of vectors. *Acta Crystallogr., Sect. A* **1978**, *34*, 827−828.
(35) Damm, K. L.; Carlson, H. A. Gaussian-Weighted RMSD Superposition of Proteins: A Structural Comparison for Flexible Proteins and Predicted Protein Structures. *Biophys. J.* **2006**, *90*, 4558−4573.
(36) Monari, A.; Rivail, J.-L.; Assfeld, X. Theoretical Modeling of Large Molecular Systems. Advances in the Local Self Consistent Field Method for Mixed Quantum Mechanics/Molecular Mechanics Calculations. *Acc. Chem. Res.* **2013**, *46*, 596−603.
(37) Boeyens, J. C. A.; Comba, P. Molecular mechanics: theoretical basis, rules, scope and limits. *Coord. Chem. Rev.* **2001**, *212*, 3−10.
(38) Echave, J.; Clary, D. C. Potential optimized discrete variable representation. *Chem. Phys. Lett.* **1992**, *190*, 225−230.
(39) Li, J.; Zeng, T.; Zhai, Y.; Qu, Z.; Li, H. Intermolecular resonance energy transfer between two lutein pigments in light-harvesting complex II studied by frenkel exciton models. *Phys. Chem. Chem. Phys.* **2023**, *25*, 24636−24642.
(40) Li, J.; Zeng, T.; Qu, Z.; Zhai, Y.; Li, H. Energy transfer from two luteins to chlorophylls in light-harvesting complex II study by using exciton models with phase correction. *Phys. Chem. Chem. Phys.* **2024**, *26*, 1023−1029.
(41) Ishikawa, H.; Field, R. W.; Farantos, S. C.; Joyeux, M.; Koput, J.; Beck, C.; Schinke, R. HCP-CPH ISOMERIZATION: Caught in the Act. *Annu. Rev. Phys. Chem.* **1999**, *50*, 443−484.
(42) Rubtsova, N. I.; Rubtsov, I. V. Vibrational Energy Transport in Molecules Studied by Relaxation-Assisted Two-Dimensional Infrared Spectroscopy. *Annu. Rev. Phys. Chem.* **2015**, *66*, 717−738.
(43) Hamm, P.; Zanni, M. *Concepts and Methods of 2D Infrared Spectroscopy*; Cambridge University Press, 2011.
(44) Kwac, K.; Lee, H.; Cho, M. Non-Gaussian statistics of amide I mode frequency fluctuation of N-methylacetamide in methanol solution: Linear and nonlinear vibrational spectra. *J. Chem. Phys.* **2004**, *120*, 1477−1490.
(45) Momma, K.; Izumi, F. VESTA3 for three-dimensional visualization of crystal, volumetric and morphology data. *J. Appl. Crystallogr.* **2011**, *44*, 1272−1276.
(46) Hirel, P. Atomsk: A tool for manipulating and converting atomic data files. *Comput. Phys. Commun.* **2015**, *197*, 212−219.
(47) Larsen, A. H.; et al. The atomic simulation environment—a Python library for working with atoms. *J. Phys.: Condens. Matter* **2017**, *29* (27), 273002.
(48) Thompson, A. P.; Aktulga, H. M.; Berger, R.; Bolintineanu, D. S.; Brown, W. M.; Crozier, P. S.; in 't Veld, P. J.; Kohlmeyer, A.; Moore, S. G.; Nguyen, T. D.; Shan, R.; Stevens, M. J.; Tranchida, J.; Trott, C.; Plimpton, S. J. LAMMPS - a flexible simulation tool for particle-based materials modeling at the atomic, meso, and continuum scales. *Comput. Phys. Commun.* **2022**, *271*, 108171.
(49) Michaud-Agrawal, N.; Denning, E. J.; Woolf, T. B.; Beckstein, O. MDAnalysis: A toolkit for the analysis of molecular dynamics simulations. *J. Comput. Chem.* **2011**, *32*, 2319−2327.
(50) Bannwarth, C.; Ehlert, S.; Grimme, S. GFN2-xTB—An Accurate and Broadly Parametrized Self-Consistent Tight-Binding Quantum Chemical Method with Multipole Electrostatics and Density-Dependent Dispersion Contributions. *J. Chem. Theory Comput.* **2019**, *15*, 1652−1671.
(51) Li, J.-R.; Zhai, Y.; Qu, Z.; Li, H. ETQTE: Energy Transfer Quantum Time Evolution. https://github.com/zhaiyusci/etqte.git, accessed: 9/14/2023.
(52) Li, Y. 1d- and 2d-IR calculation in semi-classical line shape theory. Build in C++ with Python/Cython interface. https://github.com/youli-jlu/2dIR.git, accessed: 7/1/2024.
(53) Wang, Y.; Wang, F.; Zhu, G.; Quan, Q.; Lai, Z.; Meng, Y.; Fan, Y.; Yip, S.; Zhao, D.; Ho, J. C. Deconvoluting the energy transport mechanisms in all-inorganic CsPb2Br5/CsPbBr3 perovskite composite systems. *APL Mater.* **2022**, *10*, 031101.
(54) Zhu, G.; Yang, Y.; Zeng, Y.; Mu, J.; Zheng, Z.; Yu, G. High-Pressure Ultrafast Time-Resolved Far-Infrared Full-spectrum Spectroscopy with Air-Based Upconversion. 2024; https://www.researchsquare.com/article/rs-3909502/v1, accessed: 2/22/2024.
(55) Bernstein, J. Ab initio study of energy transfer rates and impact sensitivities of crystalline explosives. *J. Chem. Phys.* **2018**, *148*, 084502.
(56) Zhu, S.; Zhu, W. An Ab Initio Molecular Dynamics study of Low Temperature Effects in Crystalline α-HMX. *Phys. Status Solidi B* **2019**, *256*, 1900057.

https://doi.org/10.1021/jacsau.4c00775
JACS Au 2024, 4, 4455−4465